Ocean Sci. Discuss., 6, 2389–2421, 2009
www.ocean-sci-discuss.net/6/2389/2009/

Ocean Science Discussions

Papers published in *Ocean Science Discussions* are under open-access review for the journal *Ocean Science*

Seasonal cycles of mixed layer salinity and evaporation minus precipitation in the Pacific Ocean

F. M. Bingham[1], **G. R. Foltz**[2], **M. J. McPhaden**[3], **and T. Suga**[4]

[1]Center for Marine Science, University of North Carolina Wilmington, 601 S. College Rd., Wilmington, NC 28403-5928, USA
[2]Joint Institute for the Study of Atmosphere and Ocean, University of Washington, 3737 Brooklyn Ave NE, Box 355672, Seattle, WA 98105-5672, USA
[3]NOAA/Pacific Marine Environmental Laboratory, 7600 Sand Point Way NE, Seattle, WA 98115, USA
[4]Department of Geophysics, Faculty of Science, Tohoku University, Aoba-ku, Sendai, 980-8578, Japan

Received: 24 August 2009 – Accepted: 2 October 2009 – Published: 26 October 2009

Correspondence to: F. M. Bingham (binghamf@uncw.edu)

Published by Copernicus Publications on behalf of the European Geosciences Union.

Abstract

The seasonal variability of mixed-layer salinity (MLS) is examined in the Pacific Ocean between 20° S and 60° N using a variety of data sources. Significant seasonal cycles were found in 5 regions: 1) the western North Pacific, 2) the northeastern North Pacific and Alaska gyre, 3) the intertropical convergence zone (ITCZ) 4) an area of the central North Pacific north of the Hawaiian Islands, 5) the central south Pacific along 10–20°S. The phase and amplitude of the seasonal cycle were determined. Amplitudes range from 0.1 to >0.5. The largest amplitudes are in the tropical band and the western North Pacific. Maximum salinity is obtained in late (northern) winter in the western North Pacific, late winter and early spring in the northeastern North Pacific, early summer in the ITCZ area, late summer and early fall in the central North Pacific area and (northern) summer in the central South Pacific. Large areas of the North and Tropical Pacific have no significant seasonal variation in MLS.

Seasonal variability of evaporation rate, precipitation rate and the difference between them (E-P) were calculated from the OAFlux and Global Precipitation Climatology Project datasets. Typical amplitudes of E-P are $0.1–1\times10^{-4}\,\mathrm{kg\,m^{-2}\,s^{-1}}$. The seasonal variability of E-P is largely dominated by variability in evaporation in the western North Pacific and precipitation elsewhere. The largest amplitudes are in areas along the edge of the western North Pacific and in the far eastern tropical Pacific around 10° N. Phases in these areas indicate maximum E-P in mid- to late winter in these areas of large amplitude. The closest correspondence between E-P and MLS is in the ITCZ.

Some terms of the MLS balance were calculated, and found to have similar magnitudes, but very different distributions. Averaged over large areas in the western North Pacific, ITCZ, South Pacific and northern North Pacific, the seasonal cycle is a balance between changes in MLS, E-P, and entrainment, with advection playing a relatively minor role.

This work highlights the potentially significant role of surface salinity in the hydrologic cycle and in subtropical mode water formation. It can also help to interpret measure-

OSD

6, 2389–2421, 2009

ments that will soon be available from the Aquarius and SMOS satellite missions.

1 Introduction

It has long been understood that the ocean outside the tropics undergoes a seasonal cycle in surface temperature, getting warmer in summer/fall and cooler in winter/spring. The reasons for this are obvious, with a strong seasonal signal in solar radiation. Seasonal changes in surface salinity (MLS) over the open ocean are much less understood. MLS in the ocean is controlled by evaporation, precipitation, entrainment, advection and mixing (Delcroix et al., 1996). Any one of these components might be expected to have seasonal variability, especially precipitation or evaporation. We would most expect to see seasonal signals in MLS in areas that have seasonal signals in evaporation and precipitation, such as areas of mode water formation and near zones of seasonally varying rainfall like the intertropical convergence zone (ITCZ).

The mode water formation process has been described in a number of places (e.g. Hanawa and Talley, 2001). It is thought to be largely a result of evaporative cooling and thickening of the surface mixed layer in wintertime. Evaporation leads not only to cooling, but also to salinification, which in turn leads to increased density. It is thus important in understanding mode water formation how much of a role is played by temperature and how much by salinity. Quantifying the seasonal cycle of salinity in mode water formation regions can help to clarify the role played by salinity and evaporation in the mode water formation process.

There are significant uncertainties in evaporation and precipitation over the ocean. Since oceanic evaporation and precipitation are important parts of the hydrologic cycle, quantifying them can help us to understand the global hydrologic cycle and its relation to climate. MLS may be controlled by evaporation and precipitation on the seasonal timescale. So understanding seasonal variation of MLS can help quantify seasonal variations in evaporation and precipitation, or more specifically evaporation minus precipitation (E-P).

OSD
6, 2389–2421, 2009

In the near future, two satellite missions, Aquarius (Lagerloef et al., 2008) and SMOS (Soil Moisture and Ocean Salinity; Berger et al., 2002) will be launched to measure surface salinity from space. To better understand satellite retrievals, it will be necessary to know the seasonal cycle of surface salinity as these will be among the earliest signals to emerge from the satellite datasets. Areas with large amplitude seasonal variability are good candidates for intensive calibration and validation activities for the missions.

The seasonal variability MLS has been most intensively studied in the tropical Pacific (e.g. Delcroix et al., 1996; Delcroix and Henin, 1991 (Henceforth DH91); Delcroix et al., 2005). DH91 looked at seasonal variability averaged from bucket data along a series of volunteer observing ship tracks in the tropical Pacific. They found maximum variability in the ITCZ in the Northern Hemisphere and along 8–10° S in the Southern Hemisphere, with SSS minima in September–October and March–April, respectively. The method they used to determine the seasonal cycles was to find the standard deviation for each month away from the mean yearly values for a particular latitude. The maximum standard deviations they found were 0.1–0.2 increasing in size and latitude from west to east. They calculated the seasonal cycles of precipitation for each of the lines to understand the relationship between rainfall and SSS. They found, as expected, that the maximum in precipitation in the South Pacific and ITCZ led the minimum in MLS by three months, leading them to conclude that the seasonal cycle in those areas was largely driven by precipitation. There was a strong maximum in the seasonal cycle along their eastern track north of the equator, near 90° W. They attributed this maximum to a combination of precipitation, evaporation and horizontal and vertical advection of salt. They discussed the role of advection of salt in the seasonal SSS budget and concluded that they did not have sufficient information to make any judgment on the importance of geostrophic advection. Seasonal Ekman advection was thought to be consistent with rainfall in its effects. DH91 examined seasonal cycles of MLS along some specific lines in limited areas, but did not include any estimate of the uncertainty of their calculations. Nevertheless, their results are largely consistent with what we will show in this paper over a much larger area.

OSD

6, 2389–2421, 2009

Delcroix et al. (1996) also examined seasonal variations of MLS and compared them with precipitation measurements. They decomposed the basin-wide MLS data into ENSO-scale first mode and seasonal second mode empirical orthogonal functions (EOFs). The seasonal mode accounted for 17% of the variance. The seasonal mode (their Fig. 6) included a maximum in variability at close to 10° N in the eastern tropical Pacific, trending toward the equator towards the west. A much stronger and oppositely-phased maximum was observed in the South Pacific at around 15° S, 170° W. At the same time, they found a similarly-structured first mode EOF in precipitation. The precipitation EOF led the (negative of the) MLS EOF in phase by about 2 months, with the precipitation reaching a minimum in July-August and the SSS a maximum in September-October. Their conclusion was that precipitation was the most important process governing MLS in the tropical Pacific. However, a spatial offset in the peaks of MLS and precipitation variability in the South Pacific implied that precipitation was not the only process controlling MLS on the seasonal time scale.

The results of Delcroix et al. (1996) are dependent upon the use of EOFs which unify the entire tropical Pacific basin. A more simple-minded analysis is attempted here assuming no connection between MLS variations in the various areas of the tropical and North Pacific. We attempt to find the phase and amplitude wherever a significant signal may exist.

Delcroix et al. (2005) examined the seasonal cycle along a number of repeating volunteer observing ship tracks in the Pacific (and Atlantic and Indian) Ocean using mainly VOS data. They found that the seasonal cycle was most pronounced in the area under the ITCZ, accounting for over 50% of the variance in this latitude band. Their analysis focused on only the latitudes equatorward of 30° and only on the MLS itself, not on the evaporation and precipitation. We will do a similar analysis here, only in a larger area of the tropical and mid-latitude Pacific from 20° S to 60° N. We will also evaluate the contribution of E-P.

In the Atlantic, Foltz and McPhaden (2008) calculated the salinity balance in three large areas, one in the central North Atlantic with weak seasonal variability and two in

the tropical and western North Atlantic with larger seasonal variability. Their approach was to use large boxes and calculate mixed-layer salt budgets. They found that the contributions to the budgets were quite varied. In the central tropical Atlantic, the seasonal cycle of MLS was mainly influenced by seasonal variation in precipitation driven by migration of the intertropical convergence zone. In the western tropical Atlantic, salinity advection was the dominant process. In the central North Atlantic, a weak seasonal cycle in MLS was mainly a balance between advection and precipitation.

Johnson et al. (2002) calculated horizontal divergence of SSS in the global tropics in the mean and on a seasonal time scale using the 1994 World Ocean Atlas (Levitus et al., 1994) and the OSCAR surface currents (Bonjean and Lagerloef, 2002). They found the seasonal divergence to be a significant fraction (53%) of the annual mean divergence. The calculation was done using a relatively large smoothing scale (9.8° longitude, 2.3° latitude) and did not include local salinity change or E-P on the seasonal scale. They did find seasonal variations in the divergence in the tropical oceans, especially underneath the ITCZ.

In the most comprehensive study of seasonal variability of MLS, Boyer and Levitus (2002) published maps of seasonal cycles on a global scale based on the 1998 World Ocean Atlas monthly gridded values (Boyer et al., 1998). The results they found are similar to what we will show in the Pacific. Our work is different from theirs in a couple of ways. Boyer and Levitus did not attempt to apply harmonic analysis to individual data, but to monthly gridded values. Thus they may have lost some of the smaller scale detail in the amplitudes and phases. They did not show the statistical significance of the harmonic amplitudes. Just as important as the amplitude and phase of the seasonal cycle is to determine the places in the ocean where seasonal cycles do not exist or cannot be determined by current data. A significant number of new data have been collected since their work, mainly through profiling floats, that are incorporated here. Finally, they did show the seasonal cycles of E-P, which we will repeat in the Pacific here, but did not estimate the advection, which we will attempt as well.

Until recently, the seasonal variability of SSS has been difficult to quantify over the

OSD

6, 2389–2421, 2009

open ocean. Salinity measurements have been limited to specific locations or ship tracks, and coverage over the entire range of seasons has been limited. Recently however, the Argo program (http://www.argo.net) has deployed profiling floats which measure profiles in random locations over a wide area. Now that Argo has been running for several years it has become possible to use these and other observations to examine variability on many time scales. As several realizations of the annual period have been measured, we can now determine the seasonal cycle of salinity and E-P, and explicitly determine the amplitude and phase and their statistical significance. Since the data are available, we take the approach of not averaging over a set of large boxes (Foltz and McPhaden, 2008), using EOFs (Delcroix et al, 1996), gridded climatologies (Boyer and Levitus, 2002) or of focusing on specific ship tracks (DH91) but of looking at the seasonal cycle in detail over a large area. This allows us to get a closer picture of areas of interest like the mode water formation regions and the ITCZ. We also examine terms of the MLS budget to see what the balance is on a seasonal time scale.

In this paper we have focused on the Pacific basin between 20° S and 60° N. There are a couple of reasons for this. There is a large concentration of MLS data in the region, from volunteer observing ship lines, Japanese hydrographic surveys, Argo floats and other sources. There have been some previous studies of seasonal variability of MLS in the region, and we are building from those to provide a regional focus and to put the previous studies in a basinwide perspective.

2 Data and methods

The data used in this study depict three different phenomena, MLS, evaporation and precipitation. In addition, for our calculations we have used mixed-layer depth (MLD) and current data to determine seasonal cycles of some of the terms in the surface salt balance. We now describe the origin and methods used for each dataset.

OSD
6, 2389–2421, 2009

2.1 Data sources

The following describes the sources for the MLS, mixed-layer depth, precipitation, evaporation and surface current data. Since each of the sources are averaged onto a slightly different grid, all datasets were subsampled or averaged onto a common 2.5°×2.5° grid.

2.1.1 Mixed-layer salinity

The MLS data used in this study come from several sources, the 2005 World Ocean Database (WOD05), EPIC CTD data, French LEGOS data, Argo and the TAO-TRITON moorings.

2.1.2 WOD05

The WOD05 (Johnson et al., 2006) contains several data files in the Pacific. In this paper we used the ocean station data (Fig. 1c; OSD), CTD and profiling float (Fig. 1d; PFL) files. The profiling float file consists mostly of Argo data (www.argo.net). For each profile in each of these files, we picked out the topmost value of salinity as the value of MLS, as long as that value was at 10 m or shallower and the observation was flagged as good in the file. No further quality checks were carried out on these data, but specific points were discarded if it became apparent in subsequent analysis that they were problematic. The distribution of the OSD data in Fig. 1c indicates that they are heavily concentrated in coastal areas near the US in the eastern Pacific, Japan in the western, and a few other areas.

2.1.3 LEGOS

The LEGOS (Laboratoire d'Etudes Geophysiques et Oceanographiques Spatiales) validated data include surface bucket and underway thermosalinograph data from 30° S–30° N in the Pacific (Fig. 1b; http://www.legos.obs-mip.fr/en/observations/sss/datadelivery/products/). These observations are heavily grouped along major shipping

OSD
6, 2389–2421, 2009

lanes. See Delcroix et al. (2005) for discussion of data origin and validation procedures. The depths represented by these data range from the surface using a bucket to a few meters from a thermosalinograph. No adjustment was made in this study for variations in sample depth or collection method. Delcroix et al. (2005) subtracted 0.1 from all bucket salinities and added 0.02 to all thermosalinograph measurements to account for the different techniques.

2.1.4 EPIC

EPIC is the data management system for oceanographic data taken during various NOAA cruises. (http://www.epic.noaa.gov) From this system, we extracted CTD data from our Pacific domain at 5 m depth. The cruises where these data were taken were mostly servicing missions for the TAO array. The number of data from this source was small compared to other sources.

2.1.5 Argo

Argo profiles were gathered from the NODC Argo data repository website (http://www.nodc.noaa.gov/argo/). Argo data from January 2004–May 2009 are used in this study with quality control flags of either 1 or 2. There is some overlap during 2004 with the WOD05 PFL data. The Argo data added about 6500 unique observations to the ensemble. Argo data have the advantage over the other datasets in that the spatial distribution is quite uniform (Fig. 1d).

2.1.6 Combined data

Once the above four datasets were extracted, they were combined into one large ensemble, taking care to screen for duplicates. There was considerable duplication, especially between the LEGOS and OSD data. The final dataset is made up of approximately 780 000 measurements between 20° S and 60° N (Fig. 1a). The distribution of observations in time (Fig. 2) shows them to be relatively uniform during the 70's and

80's, with a dip in the 90's and then another rise after 2002 with the onset of Argo sampling. Before the 90's the data consist mainly of a combination of LEGOS and OSD. In more recent times, the data are dominated by PFL/Argo. The reduction in data availability in the late 90s probably reflects delays by research institutions in submitting their data to their respective national data centers, which then submit them to the US National Oceanographic Data Center which produced the WOD05.

Each data source has a different method of measuring salinity and verifying its accuracy. In some cases (Argo, LEGOS and TAO-TRITON), the data were collected by single agencies or entities with relatively standardized techniques. The WOD05 however, is a compendium of data collected by a myriad of sources. Given the diversity of data sources, the large amount of data that were eventually used and the purpose, to calculate the seasonal harmonic, a unified approach to quality control was not possible or necessary. We adopted the data deemed acceptable by the providers' quality flags (when available), and rejected data that in subsequent analysis were obviously erroneous.

2.1.7 TAO/TRITON moorings

A separate independent analysis was carried out using near-surface TAO mooring data. The near-surface instruments typically were deployed at a depth of 1 or 2 m. Salinities were extracted from the files where the quality flag provided by the TAO program was either 1 ("highest quality") or 2 ("default quality").

2.1.8 Surface freshwater fluxes

Surface freshwater flux data were extracted from two different sources, OAFlux and GPCP.

OSD
6, 2389–2421, 2009

2.1.9 Evaporation

Evaporation data were taken from the OAFlux dataset of Yu et al. (2008; see also http://oaflux.whoi.edu/). This dataset combines satellite retrievals with three reanalyses as input to the COARE 3.0 bulk algorithm (Fairall et al., 2003). The data include monthly values of evaporation from 1958–2006 in 1° squares. Yu et al. published maps of standard deviation for latent heat flux (their Fig. 17), showing values between about 2 and 26 $W m^{-2}$. Translated into evaporation this range is $9–90 \times 10^{-7}$ $kg m^{-2} s^{-1}$, well below the amplitudes that will be calculated later in this paper.

2.1.10 Precipitation

Precipitation data were taken from the Global Precipitation Climatology Project (GPCP; http://precip.gsfc.nasa.gov/) monthly merged precipitation analysis (Huffman et al., 1997; Adler et al., 2003) on a 2.5°×2.5° grid. Adler et al. published error fields for the precipitation, and included one example month. The error fields were not used in this study, but significance estimates were based on scatter from harmonic fits (Sect. 2.2).

2.1.11 Mixed-layer depth

Mixed-layer depths were obtained from the Ocean Mixed Layer Depth Climatology (http://www.locean-ipsl.upmc.fr/~cdblod/mld.html) which is a monthly climatology of mixed-layer depth derived from World Ocean Database and World Ocean Circulation Experiment data. The climatology uses a temperature criterion of 0.2°C difference from the surface to estimate the depth (de Boyer Montegut et al., 2004). Note that this is not a time series, but a seasonal climatology, with a single value for each month for each 2° square.

OSD
6, 2389–2421, 2009

2.1.12 Surface currents

Surface currents are taken from the OSCAR current database (http://www.oscar.noaa.gov/). Currents are estimated in 1° bins from satellite altimetry and vector winds, validated from in situ sources where available (Bonjean and Lagerloef, 2002). Currents include both geostrophic and Ekman components.

2.2 Harmonic analysis

The simple harmonic analysis used in this paper closely follows the method of Emery and Thomson (2001; 392–395). For MLS for example, the combined data (Sect. 2.1.6) were grouped into boxes. For each box, MLS was least squares fit to the function

$$S = S_0 + a_0\cos(\omega t) + a_1\sin(\omega t) + \varepsilon \quad (1)$$

where $\omega = 2\pi/365.25$ days. ε is a residual whose size is minimized in a least squares sense by choice of a_0 and a_1. t is the time measured in days from January 1 of each year. The significance of the fit was determined using a standard f-test and considered significant when it exceeded 95%. The percent of variance explained by the fit (r^2) was determined as well. The amplitude of the seasonal cycle is $A = \sqrt{a_0^2 + a_1^2}$ and the phase in radians is $\phi = \tan^{-1}(a_1/a_0)$. Only the first harmonic – one cycle per year – is included in the analysis presented in this paper. We tried the same set of calculations including the semi-annual harmonic in the least squares fit as well. The results were not much different. Some areas with significant seasonal cycles got a bit larger, but the extra harmonic did not make much difference to the basic results that will be presented.

OSD
6, 2389–2421, 2009

3 Results

3.1 Seasonal cycles of MLS and E-P

The amplitude of the seasonal cycle of MLS is generally between 0.1 and 0.5 (Fig. 3) in areas where it is significant. There are roughly four areas where a significant fit was obtained: An area stretching around the northern and western rim of the North Pacific (area NWP), a band going across the tropical Pacific from close to the equator in the west to about 10° N in the east (area TP), an area in the tropical South Pacific around 10° S (area SP) and a small area north of the Hawaiian Islands centered at about 30° N (area HI). The amplitudes reach 0.5 and over in the eastern Pacific, the East China Sea and the Arafura Sea between New Guinea and Australia. Most squares with significant fits had amplitudes between 0.1 and 0.3. There are large areas of the Pacific where there were data, but no significant seasonal cycle of MLS.

The phase (Fig. 4) shows the distinction between each of the areas mentioned above. In area NWP, the maximum salinity occurs in late winter or early spring. In area TP, the maximum occurs in mid-summer. In area SP, the maximum occurs mostly in late winter/early spring (August/September), but the timing is quite variable. In area HI, the maximum occurs in the late summer and fall.

The percent of variance (Fig. 5) of squares with a significant fit ranges from 10–20% up to nearly 100%. Area TP shows the highest percent of variance explained indicating that the seasonal is the main component of MLS variation in this area. Other areas with high values of percent of variance are south of the Aleutian Islands, and the marginal areas of the Sea of Japan and the Timor Sea.

For area TP, the results closely match those of Delcroix et al. (2005) and Delcroix et al. (1996). In particular Delcroix et al. (2005) show an area of high R-squared in the eastern tropical Pacific, centered near 10° N and an area of good fit in the western tropical North Pacific, nearer to the equator. In both cases, the month of maximum salinity found here agrees with that shown by Delcroix et al. (1996) Amplitudes found here appear to be somewhat less than those found by Delcroix et al. In our results

OSD
6, 2389–2421, 2009

the western tropical Pacific, the salinity varies in almost opposite phase to the central Pacific. The month of maximum salinity is near July around 180°, and moves toward earlier in the year both to the east and west of there. In agreement with this, Delcroix et al. (1996) show an area in the western Pacific of nearly opposite phase. Gouriou and Delcroix (2002) also found similar results when they examined MLS variability in this region (10–25° S–160° E–140° W). They found a seasonal mode with an amplitude of about 0.5 pss and maximum salinity in September.

The results presented here also match with those of Hires and Montgomery (1972) who measured seasonal variability along a track from Honolulu to Pago Pago. This track crosses the equator at approximately 165° W and slopes northeastward toward Honolulu at 158° W. They found a maximum amplitude of MLS seasonal variability at about 10° N. The minimum salinity comes in November and the amplitude is about 0.6.

For the northeastern Pacific, there are almost no published reports describing SSS seasonal variability. The only related study the authors could find was that of Woodgate et al. (2005) who examined variability at a set of moorings in the Bering Straits. They observed significant seasonal variability in the SSS, with a maximum value in early spring and an amplitude of about 0.5. This is similar to what is shown in this report, but the closest observations used here are well to the south of the Bering Straits. The Coast Guard (1982) showed semi-annual variability in SSS at Ocean Station November (30° N, 140° W) from July 1966–June 1974. However, no attempt was made in that study to assess the significance of the signal. Xie and Arkin (1997) show global maps of seasonal precipitation based on the algorithm of Xie and Arkin (1996) over the years 1979–1995. Their maps show that the Alaskan gyre and northeast Pacific do get a large seasonal cycle in precipitation, with maximum rainfall in the January–March time period. This is inconsistent with the findings presented here (Fig. 4) where maximum salinity is seen in this area during March–May.

Seasonal cycles calculated from TAO moorings are similar to those from the station/float data (Figs. 3a, 4a and 5a). Significant seasonal variability is found throughout the tropical Pacific, with larger amplitudes in the northeastern area under the ITCZ.

OSD
6, 2389–2421, 2009

The maps of E-P, E and P shows that most of the Pacific has significant seasonal variability in at least one of these quantities (Fig. 6). The seasonal cycle of E-P consists of the combined seasonal cycles of E and P. The seasonal cycle of E is the dominant component in the western North Pacific, while P is generally dominant elsewhere. The areas with the maximum amplitude of E-P are in the western North Pacific near Japan and to the east, an area east of the Philippines, an area between New Guinea and Australia and an area along the ITCZ at ~10° N.

The phase of E-P (Fig. 6b) indicates the month of maximum E/minimum P. This occurs in mid-winter near Japan, in spring along the ITCZ and in southern hemisphere late winter in the western South Pacific. In a regime where MLS variability is dominated by E-P, we would expect approximately a three month time lag between the maximum of E-P and the maximum of MLS (Fig. 4a). This is more or less the case in most areas where seasonal cycles of both quantities exist. The phase of E shows maximum values throughout the North Pacific in late fall/early winter. The phase of P is more complicated, with a band across the tropical Pacific around 10° N with maximum precipitation in late summer/early fall.

3.2 Seasonal balance of MLS terms

Ignoring entrainment and turbulent vertical diffusion, a simple equation describing MLS is given by Delcroix et al. (1996)

$$\frac{\partial S}{\partial t} = \frac{S_0(E-P)}{h} - u \cdot \nabla S \tag{2}$$

where S_0 is the yearly average MLS and h is the mixed layer thickness. Each of the terms in this equation can be expressed in terms of the seasonal harmonic as in Eq. (1). In the third term, $u \cdot \nabla S$, we can express each of u and S as a mean ($\bar{u}$) and seasonally varying (u') part. The term can then be broken up into 1) seasonal advection of the mean salinity ($u' \cdot \nabla \bar{S}$), 2) mean advection of the seasonally varying salinity ($\bar{u} \cdot \nabla S'$), and 3) seasonal advection of the seasonally varying salinity ($u' \cdot \nabla S'$). We will make

OSD
6, 2389–2421, 2009

no attempt here to depict 2) and 3). Calculation of these requires computation of the spatial gradient of salinity as a function of time, and then fitting those gradients to a sinusoidal function (as in Eq. 1). We deemed that doing that with the current dataset was not possible with any degree of confidence in the results, especially with Argo data which are collected in random times and places. We do show the amplitude of and phase of 1) (Fig. 7) which exists only areas where there is a significant seasonal cycle of current. The only area where this quantity has a large value is in the northeastern North Pacific where there is a strong mean salinity gradient across the western edge of the California Current.

The map of the amplitude of the seasonal cycle of MLS (Fig. 3a) is the same as the map of the amplitude of the seasonal cycle of $\frac{\partial S}{\partial t}$ but with a different scale (Fig. 7c). The phase of $\frac{\partial S}{\partial t}$ is the same as that of S (Fig. 4a), but shifted backward in time by 3 months (Fig. 8).

The seasonal cycle of the $\frac{S_0(E-P)}{h}$ term of (2) (Fig. 9) largely follows E-P (Fig. 6a,b). It is strongest under the ITCZ in the eastern tropical North Pacific where it is driven by seasonal variations in rainfall, and in the western North Pacific where evaporation is the dominant process. Comparison of the figures showing the terms of Eq. (2) (Figs. 3a, 7, 8 and 9) indicate some rough agreement between them in amplitude and phase. In areas where there is a significant seasonal cycle of $\frac{\partial S}{\partial t}$ it matches or nearly matches that of $\frac{S_0(E-P)}{h}$. In the northeastern North Pacific, there is a small area where the advection term is strong, but the phase is noisy. In that area, $\frac{S_0(E-P)}{h}$ does not have an amplitude nearly as large as advection. Exactly how the seasonal balance of MLS works at the offshore edge of the California Current is unclear.

To get a better sense of the seasonal cycle on a regional scale, we calculated it over some larger areas as shown in Fig. 10, with results displayed in Table 1. In all the areas shown except the South Pacific the amplitude and phase of the $\frac{S_0(E-P)}{h}$ and $\frac{\partial S}{\partial t}$ terms are similar. Phases are within two months and amplitudes within $1–2\times10^{-8}$ pss s^{-1}, indicating rough balance between the terms. The tropical South Pacific area is the

OSD
6, 2389–2421, 2009

one where the largest discrepancy occurs, with no significant seasonal signal at all in $\frac{S_0(E-P)}{h}$. The differing natures of the seasonal cycles are illustrated in Fig. 11, in which we show all the MLS data for each area, plotted as if they were collected in a single year, with monthly averages also displayed. The seasonal cycles in the tropical North Pacific and the northern North Pacific are sinusoidal, with MLS maxima in March/April and April/May, respectively. The seasonal variations in the South Pacific and western North Pacific are more driven by a number of low outliers in the summer season in each case, giving maximum MLS values in the winter.

4 Discussion

The phase-locked seasonal variability of MLS in the Pacific has been studied, using MLS and E-P data along with surface currents and mixed-layer depths. By phase-locked, we mean variability that is tied to the season as long as data have been available to measure it. This is opposed to variability at the seasonal time scale with random phase such as might be measured using spectral analysis. Maps of MLS seasonal cycles show limited areas where they are significant and large areas of the central oceans where they are not. Nevertheless, we were able to quantify and characterize the variability in the areas where it was most obvious, the western North Pacific boundary and mode water formation area, underneath the ITCZ in the eastern tropical Pacific, in the low-latitude eastern South Pacific, and in the northern North Pacific. In many areas, there is a seasonal balance between E-P and changing MLS.

Large amplitude changes in MLS in the mode water formation area of the western North Pacific likely play a significant role in the formation process. Until now, much has been made of the way that density increases in this area in the wintertime leading to a thickening mixed-layer (e.g. Bingham, 1992). In most studies, decreased temperature has been considered as the main factor driving increased density. However, the present study suggests that seasonal variability in salinity, shown here to have just the right phase, could contribute significantly to mode water formation as well. At a base

OSD
6, 2389–2421, 2009

salinity of 35 and temperature of 15°C, a seasonal cycle of 0.5 in salinity is the density equivalent of a seasonal cycle of temperature of about 2°C. The extra densification provided by salinity may be enough to create the extremely thick mixed layers seen in this area in late winter.

Seasonal advection was seen to play a minimal role in the salinity balance. However, the difficulty of doing the calculation of the mean advection of the seasonally varying salinity makes this conclusion very uncertain. Despite this, we did show that advection may play an important role in the northeastern North Pacific at the offshore edge of the California Current. DH91 emphasized the role of meridional Ekman advection on the mean MLS, noting that the meridional maximum of precipitation is displaced slightly equatorward of the minimum of the mean MLS, attributing this displacement to advection. Delcroix et al. (1996) briefly discussed the potential role of seasonal advection of MLS by the north equatorial countercurrent, concluding it might possibly be significant. The value they give for the possible contribution, 25×10^{-2} month^{-1}, is approximately equivalent to 1×10^{-7} pss s^{-1} as presented here (Fig. 7). We cannot support this conclusion from the present data, the main reason being the lack of seasonal variability in the OSCAR currents in the tropics. Why the OSCAR seasonal variability contrasts so much with the results of Reverdin et al. (1994) may be the subject of a future study.

There remains the possibility that the lack of seasonal variation of salinity in large areas of the Pacific is simply due to a lack of sufficient data, and that as Argo data become more abundant, many of the gaps in Fig. 3a will be filled in and the seasonal cycle better defined. It is also possible that in some areas of the Pacific the seasonal cycle of MLS is not closed. That is, variability at a period of one year is matched by variability with some other periodicity. This may be particularly true in the tropical Pacific where the ENSO cycle is important, and also phase-locked to the calendar year (Clarke, 2008). Imbalance in the seasonal cycle may play some role in triggering ENSO events in a manner dictated by some "recharge oscillator" theories of ENSO (e.g. Jin, 1997).

This work has important implications for the SMOS and Aquarius satellite missions.

OSD
6, 2389–2421, 2009

Aquarius is supposed to deliver surface salinity measurements with accuracies of 0.1–0.2 pss with a spatial resolution of 100–300 km and a temporal resolution of 7–30 days (Lagerloef et al., 2008). There are two main areas in the Pacific with seasonal amplitudes this large and predictable phase, the ITCZ and the western North Pacific. The signals the satellite sees in these areas should be among the first to emerge from the data stream. Thus, these areas will make good test beds for the satellite missions and would be good candidates for intensive calibration and validation activities.

Acknowledgements. Argo data were collected and made freely available by the International Argo Project and the national initiatives that contribute to it (http://www.argo.net). Argo is a pilot programme of the Global Ocean Observing System.

References

Adler, R. F., Huffman, G. J., Chang, A., Ferraro, R., Xie, P., Janowiak, J., Rudolf, R., Schneider, U., Curtis, S., Bolvin, D., Gruber, A., Susskind, J., Arkin, A., and Nelkin, E.: The version 2 Global Precipitation Climatology Project (GPCP) monthly precipitation analysis (1979–Present), J. Hydrometeorol., 4, 1147–1167, 2003.

Berger, M., Camps, A., Font, J., Kerr, Y., Miller, J., Johannessen, J., Boutin, J., Drinkwater, M. R., Skou, N., Floury, N., Rast, M., Rebhan, H., and Attema, E.: Measuring ocean salinity with ESA's SMOS mission, ESA Bull., 111, 113–121, 2002.

Bingham, F.: The formation and spreading of subtropical mode water in the North Pacific, J. Geophys. Res., 97, 11177–11189, 1992.

Bonjean, F. and Lagerloef, G. S.: Diagnostic model and analysis of the surface currents in the Tropical Pacific Ocean, J. Phys. Oceanogr., 32, 2938–2954, 2002.

Boyer, T., Levitus, S., Antonov, J., Conkright, M., O'Brien, T., and Stephens, C.: World Ocean Atlas 1998 Volume 5: Salinity of the Pacific Ocean, 166 pp., Silver Spring, MD, 1998.

Boyer, T. P. and Levitus, S.: Harmonic analysis of climatological sea surface salinity, J. Geophys. Res., 107(C12), 8006, doi:10.1029/2001JC000829, 2002.

Clarke, A. J.: An Introduction to the Dynamics of El Nino and the Southern Oscillation, 308 pp., Elsevier Inc., London, 2008.

de Boyer Montegut, C., Madec, G., Fischer, A. S., Lazar, A., and Iudicone, D.: Mixed layer depth over the global ocean: An examination of profile data and a profile-based climatology, J. Geophys. Res., 109, C12003, doi:10.1029/2004JC002378, 2004.
Delcroix, T. and Henin C.: Seasonal and interannual variations of sea surface salinity in the Tropical Pacific Ocean, J. Geophys. Res., 96, C12, 22135–22150, 1991.
Delcroix, T., Henin, C., Porte, V., and Arkin, P.: Precipitation and sea-surface salinity in the Tropical Pacific, Deep-Sea Res. Pt. I, 43, 1123–1141, 1996.
Delcroix, T., McPhaden, M., Dessier, A., and Gouriou, Y.: Time and space scales for sea surface salinity in the tropical oceans, Deep-Sea Res., 52, 787–813, 2005.
Emery, W. and Thomson, R.: Data Analysis Methods in Physical Oceanography. 2nd and Revised edn., 658 pp., Elsevier Science Ltd., 2001.
Fairall, C. W., Bradley, E. F., Hare, J., Grachev, A. A., and Edson, J. B.: Bulk parameterization on air-sea fluxes: Updates and verification for the COARE algorithm, J. Climate, 16, 571–591, 2003.
Foltz, G. R. and McPhaden, M. J.: Seasonal mixed layer salinity balance of the tropical North Atlantic Ocean, J. Geophys. Res., 113, C02013, doi:10.1029/2007JC004178, 2008.
Gouriou, Y. and Delcroix, T.: Seasonal and ENSO variations of sea surface salinity and temperature in the South Pacific convergence zone during 1976–2000, J. Geophys. Res. (C Oceans), 107(C12), 3185, doi:10.1029/2001JC000830-8011, 2002.
Hanawa, K. and Talley, L. D.: Chapter 5.4 Mode Waters, in: Ocean Circulation and Climate, edited by Siedler, G., Church, J., and Gould, J., Academic Press, New York, 2001.
Hires, R. I. and Montgomery. R. B.: Navifacial temperature and salinity along the track from Samoa to Hawaii, 1957–1965, Jour. Mar. Res., 30, 177–200, 1972.
Huffman, G. J., Adler, R. F., Arkin, P. A., Chang, A., Ferraro, R., Gruber, A., Janowiak, J., Joyce, R. J., McNab, A., Rudolf, R., Schneider, U., and Xie, P.: The Global Precipitation Climatology Project (GPCP) combined precipitation data set, B. Am. Meteorol. Soc., 78, 5–20, 1997.
Jin, F. F.: An equatorial ocean recharge paradigm for ENSO. Part 1: Conceptual model, J. Atmos. Sci., 54, 811–829, 1997.
Johnson, E., Lagerloef, G. S., Gunn, J., and Bonjean, F.: Surface salinity advection in the tropical oceans compared with atmospheric freshwater forcing: A trial balance, J. Geophys. Res. (C Oceans), 107(C12), 8014, doi:10.1029/2001JC001122, 2002.
Johnson, D., Boyer, T. P., Garcia, H. E., Locarnini, R. A., Mishonov, A. V., Pitcher, M. T., Baranova, M. T., Antonov, J. I., and Smolyar, I.: World Ocean Database 2005 Documentation,

OSD
6, 2389–2421, 2009

163 pp., U.S. Government Printing Office, Washington, DC, 2006.
Lagerloef, G. S., Colomb, F. R., Le Vine, D. M., Wentz, F., Yueh, S., Ruf, C., Lilly, J., Gunn, J., Chao, Y., deCharon, A., Feldman, G., and Swift, C.: The Aquarius/SAC-D mission: Designed to meet the salinity remote-sensing challenge, Oceanography, 20, 68–81, 2008.
Levitus, S., Burgett, R., and Boyer, T. P.: World Ocean Atlas 1994 Volume 3: Salinity, 99 pp., Washington, DC, 1994.
Reverdin, G., Frankignoul, C., Kestenare, E., and McPhaden, M. Seasonal variability in the surface currents of the equatorial Pacific, J. Geophys. Res., 99(C10), 20323–20344, 1994.
Woodgate, R. A., Aagaard, K., and Weingartner, T. J.: Monthly temperature, salinity and transport variability of the Bering Strait through flow, Geophys. Res. Lett., 32, L04601, doi:10.1029/2004GL021880, 2005.
Xie, P. and Arkin, P. A.: Analysis of global monthly precipitation using gauge obseravtions, satellite estimates, and numerical moel predictions. J. Climate, 9, 840–858, 1996.
Xie, P. and Arkin, P. A.: Global precipitation: a 17 year analysis based on gauge observations, satellite estimates and numerical model outputs, B. Am. Meteorol. Soc., 78, 2539–2558, 1997.
Yu, L., Jin, X., and Weller, R.: Multidecade Global Flux Datasets from the Objectively Analyzed Air-sea Fluxes (OAFlux) Project: Latent and Sensible Heat Fluxes, Ocean Evaporation, and Related Surface Meteorological Variables, 64 pp., 2008.

Table 1. Amplitudes and phases of seasonal constituents shown in the first line in areas shown in Fig. 10. Amplitudes are in units of 10^{-8} pss s^{-1}. Phases are in months, 1=1 January, 2=1 February, etc., and indicate the month of maximum value. Phase values in parentheses are dates of maximum salinity in each area and correspond approximately with the peaks of the curves in Fig. 11. Error bounds represent 95% confidence intervals found through a propagation of errors calculation.

Area	$\frac{dS}{dt}$ Amplitude	$\frac{dS}{dt}$ Phase	$S_0\frac{(E-P)}{h}$ Amplitude	$S_0\frac{(E-P)}{h}$ Phase
Northern Tropical Pacific	7.1±0.2	1.29 (4.29)±0.07	7.0±0.1	2.88±0.03
Western North Pacific	4.5±0.1	11.99 (2.99)±0.04	4.9±0.1	12.74±0.04
Southern Tropical Pacific	2.8±0.1	7.03 (10.03)±0.10	Not significant	Not significant
Northern North Pacific	2.9±0.2	1.17 (4.17)±0.14	3.15±0.05	1.98±0.03

OSD
6, 2389–2421, 2009

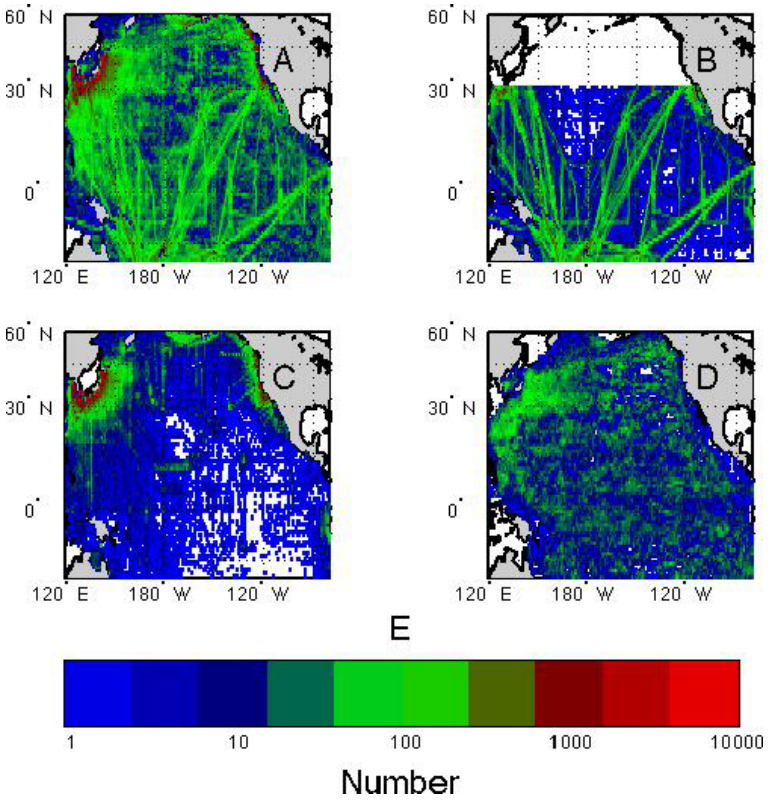

Fig. 1. Spatial distribution of MLS observation density, number of observations/1° square. **(A)** All data. **(B)** Legos Data. **(C)** OSD data. **(D)** Combined PFL and Argo data. **(E)** Color scale. Note color scale is logarithmic. Note also that there was considerable overlap between the original datasets, particularly Legos and OSD. This figure depicts the final data after removal of duplicate measurements.

OSD
6, 2389–2421, 2009

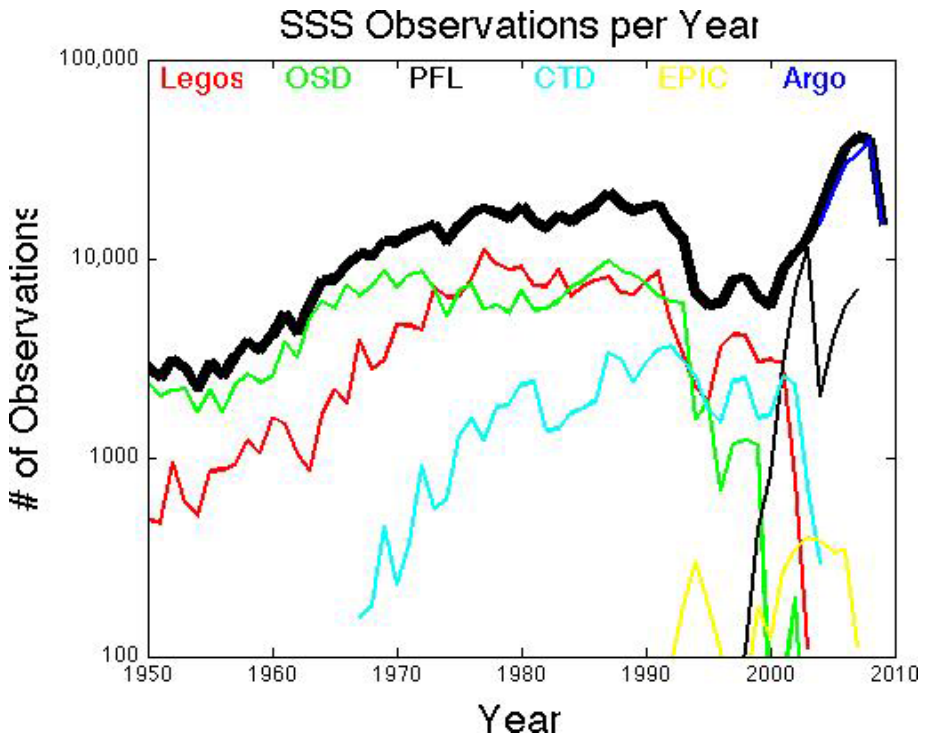

Fig. 2. Time distribution of SSS observations per year in the final dataset. Different colored lines are matched with text at the top of the figure to show which dataset is being plotted. The thick black line is the total for all observations. Note the ordinate is logarithmic. Note also that there was considerable overlap between datasets, particularly Legos and OSD. This figure depicts the final dataset after removal of duplicate measurements.

OSD
6, 2389–2421, 2009

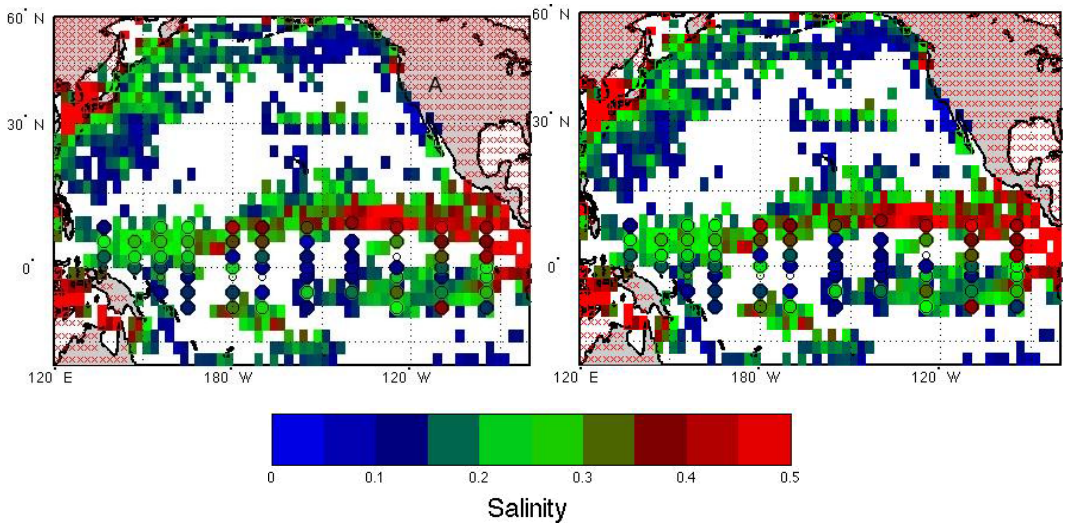

Fig. 3. (A) Amplitude of the seasonal cycle of MLS from the combined dataset. Areas with no fill had observations, but from those observations no significant seasonal component was found. Small red "x"'s indicate no data. Seasonal cycles from TAO/TRITON moorings are shown in circles near the equator. Small empty circles indicate that mooring data were examined, but no significant seasonal cycle was found for that mooring. **(B)** Color scale for panel (A), with units of pss.

OSD

6, 2389–2421, 2009

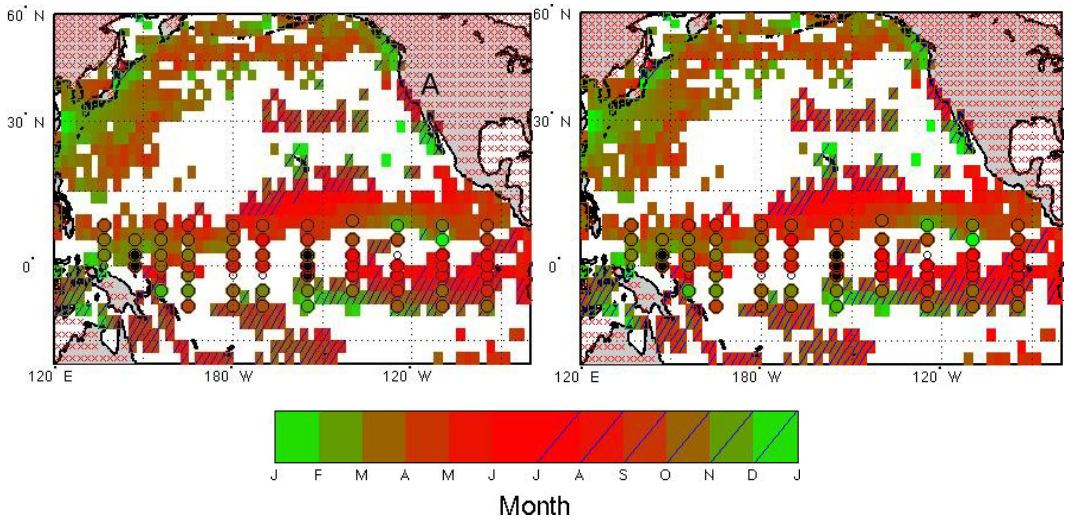

Fig. 4. (A) As in Fig. 3a, but for the phase. **(B)** Color scale for panel (A), with units of months, indicating the month of maximum MLS. Light blue slashes mean maximum MLS occurred during the second half of the year. For TAO/TRITON moorings a dark black dot in the middle indicates maximum MLS in the second half of the year.

OSD
6, 2389–2421, 2009

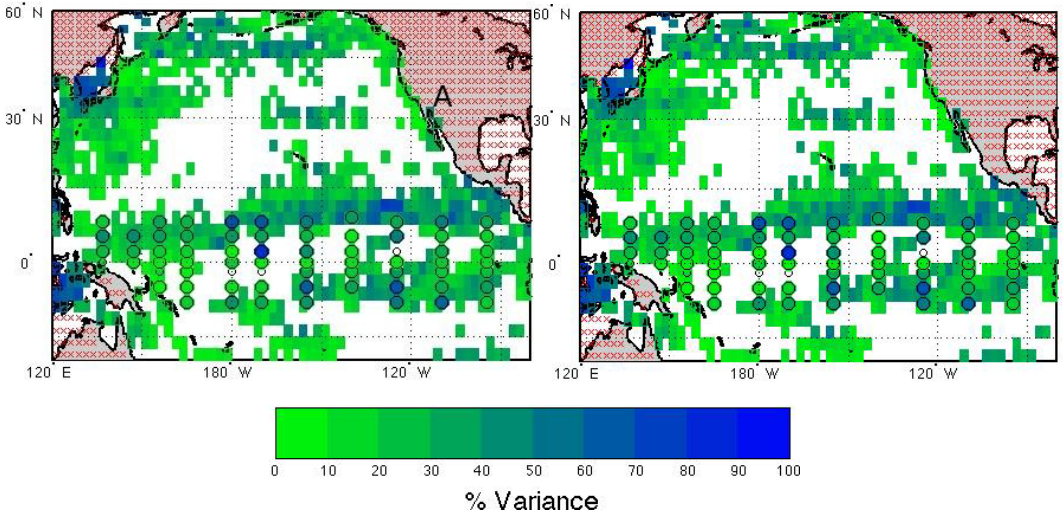

Fig. 5. **(A)** As in Fig. 3a, but for R-squared. **(B)** Color scale for panel (A), with units of %, indicating the fraction of variance explained by the seasonal cycle in each location.

OSD
6, 2389–2421, 2009

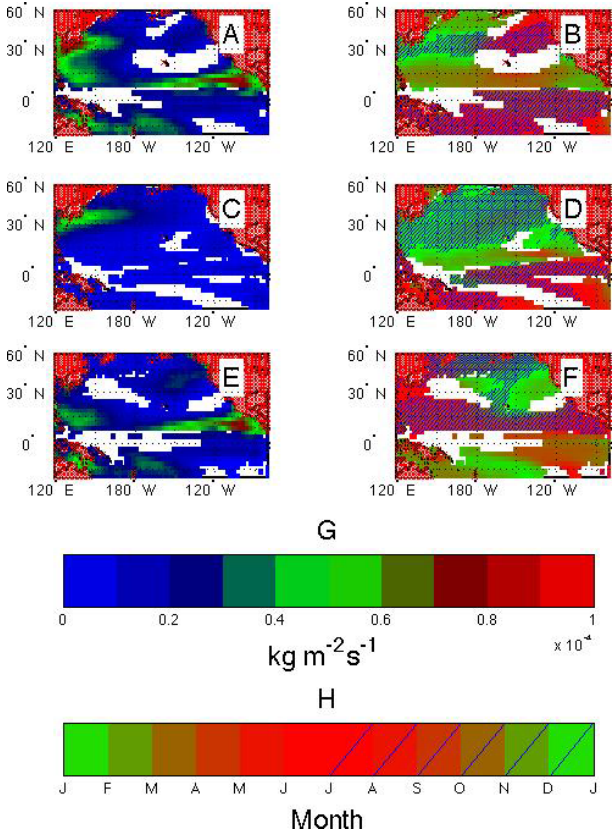

Fig. 6. Amplitude and phase of the seasonal cycle of **(A)** and **(B)** E-P, **(C)** and **(D)** evaporation and **(E)** and **(F)** precipitation. Panels (E) and (F) present the same information as Adler et al (2003) Fig. 10. **(G)** Color scale for panels (A), (C) and (E), with units of 10^{-4} kg/m^2/s. **(H)** Color scale for panels (B), (D) and (F) showing month of maximum value.

OSD
6, 2389–2421, 2009

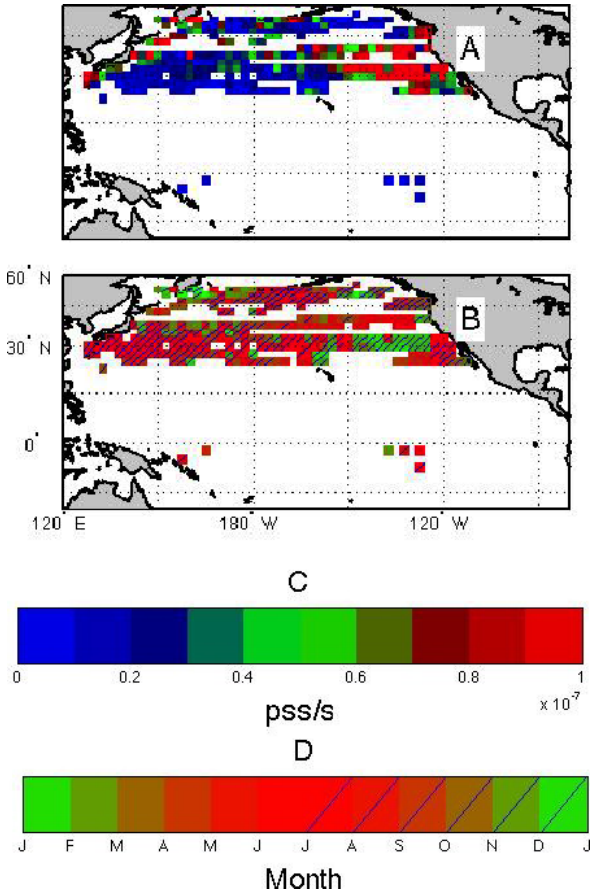

Fig. 7. **(A)** Amplitude of the $u' \cdot \nabla \bar{S}$ term in Eq. (2). **(B)** Phase of the $u' \cdot \nabla \bar{S}$ term in Eq. (2) indicating month of maximum value. **(C)** Color scale for panel (A) with units 10^{-7} pss s^{-1}. **(D)** Color scale for panel (B) showing month of maximum value.

OSD
6, 2389–2421, 2009

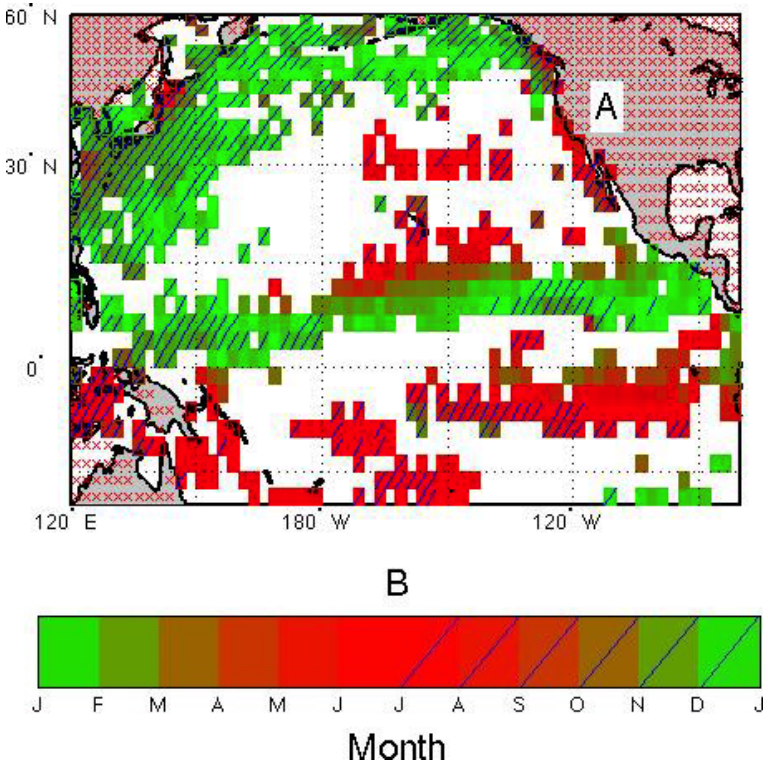

Fig. 8. **(A)** Phase of the seasonal cycle of *dS/dt* from the combined dataset. This figure presents the same information as Fig. 4a (without the TAO/TRITON data), shifted backward in time by 3 months. **(B)** Color scale for panel (A) indicating month of maximum value.

OSD
6, 2389–2421, 2009

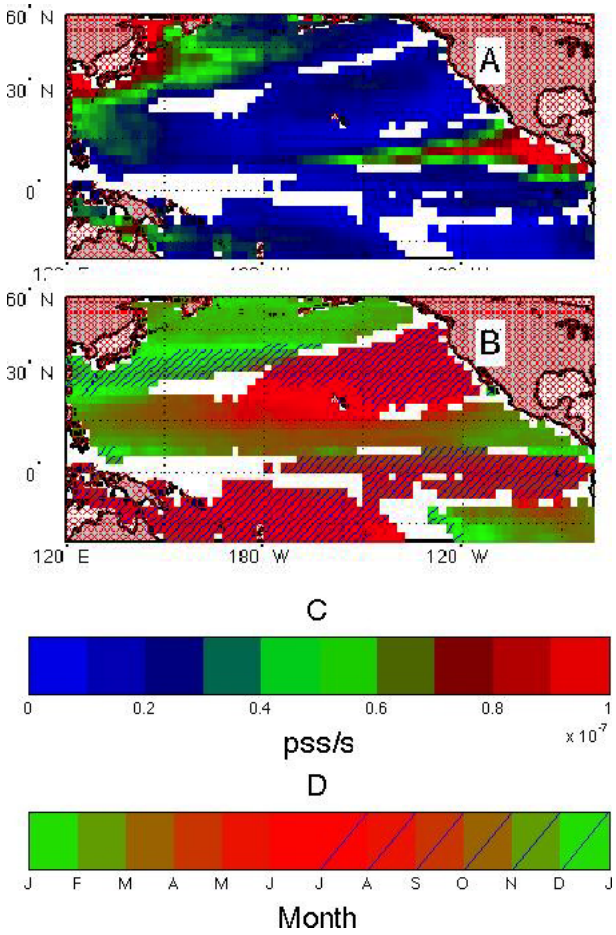

Fig. 9. **(A)** Amplitude and **(B)** phase of the seasonal cycle of $\frac{s_0(\text{E-P})}{h}$ from Eq. (2). **(C)** Color scale for panel (A) in units of 10^{-7} pss. **(D)** Color scale for panel (B) indicating month of maximum value.

OSD
6, 2389–2421, 2009

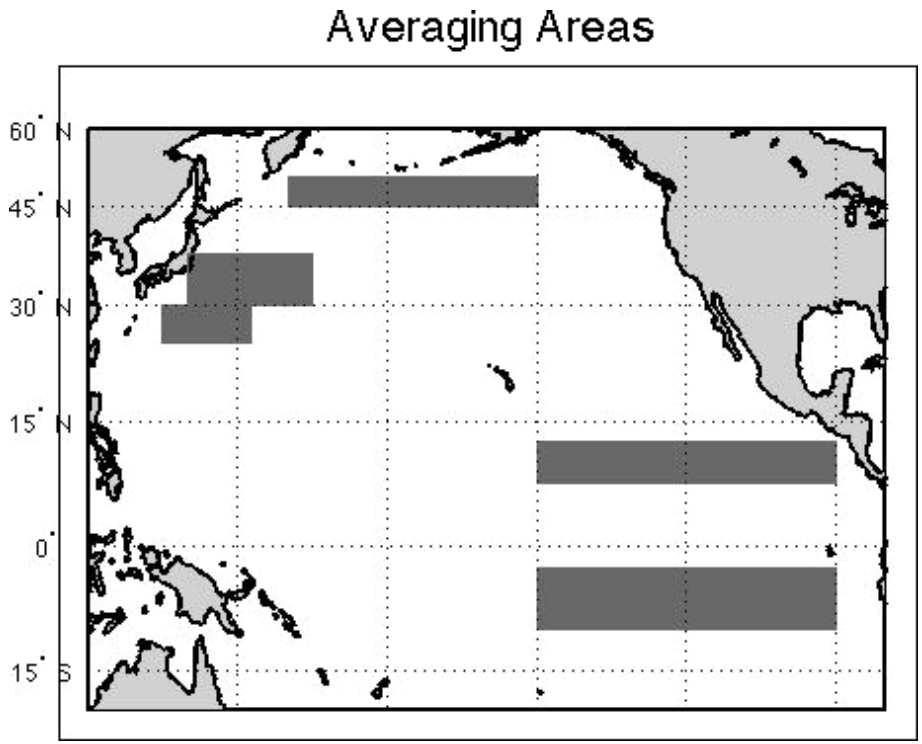

Fig. 10. Averaging areas as described in Table 1.

OSD
6, 2389–2421, 2009

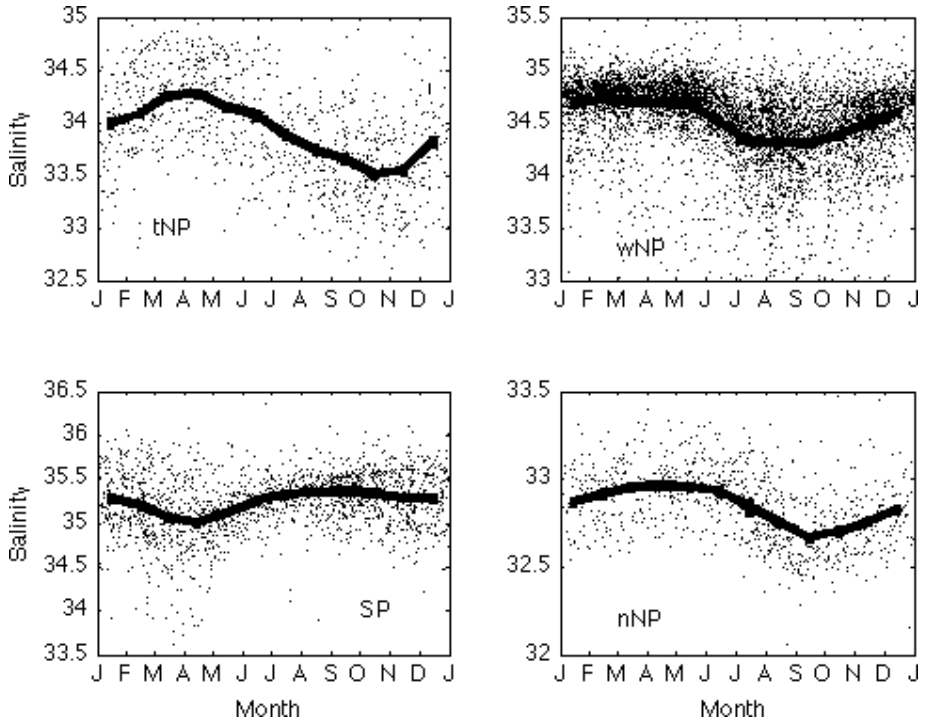

Fig. 11. MLS for the areas depicted in Fig. 10 and Table 1, plotted as a single year. Note that *y*-axis limits are different for each panel. Lettering in the bottom of each panel corresponds to areas described in Table 1. Dots are individual measurements, with only 10% of points plotted for clarity. Solid curves are monthly averages.

OSD
6, 2389–2421, 2009